Materials & Design 252 (2025) 113700

Contents lists available at ScienceDirect

Materials & Design

journal homepage: www.elsevier.com/locate/matdes

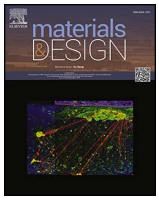

Udimet 720Li as a potential alternative for optimised aeroengine turbines: Thermophysical and thermomechanical characterisation under wide-ranging testing conditions

Gorka Ortiz-de-Zarate [a,*], Idriss Tiba [b], Aitor Madariaga [c], Arantza Linaza [d], Ainhara Garay [a], Guénaël Germain [b], Pedro J. Arrazola [a]

[a] Mondragon Unibertsitatea, Faculty of Engineering, Loramendi 4, Arrasate-Mondragón 20500 Spain
[b] LAMPA, Arts et Métiers Institute of Technology, 2 boulevard du Ronceray, Angers BP 93525-49035, France
[c] The University of Manchester, Department of Materials, Oxford Road, Manchester M13 9PL United Kingdom
[d] ITP Aero, Parque Tecnológico, Edificio 300, Zamudio 48170, Spain

ARTICLE INFO

Keywords:
Udimet 720Li
Nickel-based alloy
Thermomechanical properties
Thermophysical properties
Microstructure
Turbine

ABSTRACT

The need to reduce fuel consumption and emissions is driving advances in aeroengine performance. Efficiency gains are limited by the capacity of the turbine material to withstand the high thermomechanical loads of the combustion process. Nickel-based alloy Udimet 720Li has emerged as a promising alternative to the most widely used Inconel 718 for critical aeroengine components. Nonetheless, its material properties under industry-relevant conditions remain understudied, hindering industrial implementation. Furthermore, discrepancies in the methodology for applying adiabatic heating correction in thermomechanical tests on nickel-based alloys prevent comparability of studies and alloys. This paper presents the thermophysical and thermomechanical properties of forged and heat-treated Udimet 720Li to enable advanced aeroengine design and manufacture. A novel adiabatic heating correction procedure is also proposed for thermomechanical tests. Thermophysical properties (specific heat, density, diffusivity, thermal expansion, and conductivity) were characterised for temperatures 20–1200 °C. Thermomechanical properties were obtained for temperatures 20–1100 °C and strain rates 0.01–100 s^{-1} with cylinder compression tests. The results show that Udimet 720Li exhibits higher thermomechanical properties than Inconel 718 at elevated temperatures and can withstand greater in-service temperatures (8–23 %) due to the higher γ' strengthening phase content which remains stable up to 760 °C.

1. Introduction

The pressing need to reduce fuel consumption and lower CO_2 and NOx emissions in the aviation sector [1,2] is driving initiatives to produce more powerful and efficient engines. Increasing the Turbine Entry Temperature (TET) is considered the most suitable approach, since it raises the pressure ratio (by the ideal gas law), leading to increased efficiency in accordance with the ideal Brayton efficiency equation [3,4]. However, any increase in TET is limited by the capacity of the turbine materials to withstand the high thermomechanical loads involved in the combustion process. For this reason, heat resistant nickel-based superalloys are used to manufacture turbine components due to their excellent thermomechanical properties at elevated temperatures. In fact, the development of new heat-resistant alloys has permitted an increase in TET from ≈ 800 °C in 1940 to 1500 °C in 2010 [5], and work continues to this day.

For more than 40 years, Inconel 718 has been the most widely employed nickel-based alloy for aircraft engine components, accounting for more than 30 % of the finished component weight of a modern aircraft engine [6]. High strength, creep resistance, and good fatigue life at high temperatures makes Inconel 718 an ideal material for turbine disc fabrication [4,6–10]. However, the in-service temperature of Inconel 718 is limited to 600–650 °C in critical aeroengine components, because above this temperature its mechanical strength is drastically reduced [9]. This reduction occurs because the primary strengthening phases of this alloy (γ' and γ'') undergo a transformation at 650 °C [9,10].

New nickel-based alloys have thus been developed to withstand

* Corresponding author.
E-mail address: gortizdezarate@mondragon.edu (G. Ortiz-de-Zarate).

https://doi.org/10.1016/j.matdes.2025.113700
Received 10 September 2024; Received in revised form 20 January 2025; Accepted 5 February 2025
Available online 7 February 2025

higher temperatures than Inconel 718 [5,11]. In the 1980 s, the focus shifted to novel alloys (Rene 88, NR 3, N18, RR1000 etc.) because of their higher strength, creep, and fatigue properties in harsh environments and at higher in-service temperatures [3,12]. However, the high fraction of strengthening phase (γ') in these alloys required processing by the costly powder metallurgy route, rather than the conventional and cheaper Cast and Wrought route (C&W).

In light of these cost considerations, C&W superalloys continued to be developed in parallel, with a focus on improving the temperature capacity while maintaining good processing characteristics. Of these, the alloy Udimet 720Li (low interstitial) has emerged as a promising alternative, reaching a γ' phase volume content of ≈ 45 % [13,14], the upper limit of γ' precipitation content of C&W materials. This elevated γ' phase content is believed to contribute to superior mechanical properties at higher temperatures [15,16], outperforming alloys with lower strengthening phase content, such as the reference alloy Inconel 718 (20 %) [4,9,10].

Although Udimet 720Li has the potential to replace Inconel 718 in several turbine component applications requiring higher temperature capacities, there exists little published data on its material properties. Critically, this lack of data limits advances in the design and manufacturing route of turbines. Therefore, it is necessary to characterise the material properties not only under in-service conditions (low strain rates and in-service temperatures around 600–800 °C), but also under manufacturing conditions that include forging (low strain rates and high temperatures) and machining (high strains, strain rates, and temperatures). Gaining these insights into Udimet 720Li is crucial for the development of robust material models to simulate the various stages of the turbine disc manufacturing process, streamline turbine design, and evaluate in-service performance.

Studies of note include Aba-Perea et al. [14], who compared the diffraction elastic constants and phase specific elastic constants of Udimet 720Li and Inconel 718 at a range of temperatures (20–650 °C for Udimet 720Li and 20–750 °C for Inconel 718) and a quasi-static strain rate by combining in-situ thermomechanical tests and neutron diffraction. They concluded that the phases of Udimet 720Li (γ and γ') showed higher specific elastic constants at all tested temperatures than Inconel 718. Furthermore, their study determined comparable values for Young's moduli and Poisson's ratios between the matrix phase (γ) and the precipitation phase (γ') in Udimet 720Li. This validated the reliability of using a single-phase model fitting approach for analysing diffraction data, ensuring accurate representation of the mechanical behaviour of the material. However, as they noted, the experimental procedure did not permit an extension of the analysis to higher temperatures. This was due to the added uncertainties stemming from microstructural instability, which led to more pronounced deviations in the results at higher temperatures than in their experiments (750 °C). Moreover, although the samples were heat-treated, no forging was applied prior to testing. This is a critical consideration, as forging is a process that impacts the mechanical properties of the components used in real aeroengine applications and may not affect Inconel 718 and Udimet 720Li alloys equally.

Gopinath et al. [17] conducted tensile tests to characterise the thermomechanical behaviour of forged and heat-treated (solution treated and precipitation hardened) Udimet 720Li at quasi-static strain rates (10^{-5}–10^{-1} s^{-1}) and temperatures from 25 to 750 °C. In a further study, they conducted additional tensile tests to investigate dynamic strain ageing, using the same strain rates but a narrower temperature range of 350–450 °C [18]. Similarly, Devaux et al. [19] performed tensile tests of forged and heat-treated Udimet 720Li, AD730, Inconel 718, and Inconel 718 Plus at only three temperatures (20, 650, and 700 °C) and an unknown strain rate. Therefore, in all three cases, the results were constrained by limited temperatures and strain rates. The only published compression test results of Udimet 720Li were conducted by Wan et al. [20] and Chen et al. [13] for a range of strain rates (0.001–10 s^{-1} [20] and 0.01–0.5 s^{-1} [13]) and high temperatures (1060–1180 °C [20] and 1040–1130 °C [13]). However, the temperature range tested in these compression test works is far from the in-service thermal loads that an aeroengine turbine must withstand.

In addition to limited published data on the thermomechanical properties of Udimet 720Li, the findings in nickel-based alloy testing are often contradictory. For instance, some authors have reported strain rate softening [21,22], while others observed a hardening effect in Inconel 718 [9,23]. Additional studies have found strain softening at low temperatures [24] and at high temperatures [9,25], while other investigations did not observe any softening behaviour [21,23]. Similarly, despite the limited studies on Udimet 720Li, significant differences in trends have also been observed. Under identical conditions—strain rates of 0.01 and 0.1 s^{-1}, and a temperature of 1100 °C—some researchers reported slight strain softening [20], while others noted hardening at 0.01 s^{-1} and an initial softening followed by hardening at 0.1 s^{-1} [13]. Additionally, notable differences in flow stress values were observed. These contradictions further complicate the task of establishing a reliable comparison between Udimet 720Li and Inconel 718.

One of the main reasons for these differences is the adiabatic heating corrections applied to the stress–strain curves obtained in the thermomechanical characterisation tests, which significantly affect the results. Adiabatic heating (ΔT_{adb}) is the instantaneous temperature rise produced by the large plastic deformation of the specimen. At quasi-static strain rates ($< 10^{-3}$ s^{-1}), the process can be considered isothermal because there is sufficient time for heat dissipation [26,27]. In contrast, at higher strain rates (> 10 s^{-1}), the process is adiabatic [27]. In the intermediate range, the process is neither fully adiabatic nor isothermal. Consequently, adiabatic heating correction becomes increasingly significant at strain rates above quasi-static levels, and the requirement for its application grows as the strain rate increases. As a general rule, it is deemed essential for strain rates above 1 s^{-1} [26]. Nonetheless, some researchers have considered the effect of adiabatic heating negligible for nickel-based alloys [9,17], while others have corrected it with analytical equations [20,21], or have not mentioned it at all [19,22–24]. As a result, there is little published data investigating the influence of adiabatic heating correction for wide range of testing conditions (strain rate and temperature), and none of them for Udimet 720Li.

Most of the studies in which adiabatic heating is calculated have applied analytical methods using equation (1):

$$\Delta T_{adb} = \eta_{adb} \cdot \frac{\beta}{\rho \cdot C_p} \cdot \int_0^{\varepsilon} \sigma \mathrm{d}\varepsilon \tag{1}$$

where, η_{adb} is the adiabatic correction factor for strain rate sensitivity, β is the Taylor Quinney coefficient, ρ is the density for each temperature, C_p is the heat capacity, σ is the stress, and ε the strain. To apply this correction, it is necessary to know the thermal (heat capacity) and physical (density) properties of the material. To the best of the authors' knowledge, however, no studies have reported the properties of Udimet 720Li.

Nonetheless, this equation can only be considered an approximation since it does not consider the heat losses by conduction, convection, and radiation that may affect the calculated temperature rise [28]. It also contains certain parameters that are not typically characterised due to the difficulty involved in the experimental procedure, such as η_{adb} and β. As a result, there are significant discrepancies in the literature concerning their value. For instance, although β is generally reported to be 0.9–0.95 [29], two studies conducted on Inconel 718 observed completely different values of 0.6–0.69 [30] and 0.17–0.48 [31] in their respective works. For this reason, some researchers have proposed empirical measurement of adiabatic heating using thermocouples [32] or infrared filming [28,33]. However, this approach has not yet been applied to nickel-based alloys.

In the published data, η_{adb} commonly takes a value of 0 for isothermal conditions ($\dot{\varepsilon} \leq 10^{-3}$ s^{-1}) and 1 at fully adiabatic conditions ($\dot{\varepsilon} \geq 10^{1}$ s^{-1}). Intermediate values are generally obtained by a linear

regression between both conditions [34], and thus, in the intermediate stretch between isothermal and adiabatic conditions, the uncertainty of the method is even more significant.

Thus, this literature review would seem to indicate that Udimet 720Li is a viable alternative to Inconel 718 for improving aeroengine efficiency, however, the lack of comprehensive data on its material properties impedes the development and design of components made from this emergent alloy. The published thermomechanical properties are confined to a limited range of temperatures and strain rates. Moreover, there is no single study that characterises the thermomechanical properties of Udimet 720Li from low to high temperatures and strain rates, which would allow the development of robust material models. Existing studies focus primarily on either low (<750 °C) [14,17–19] or high temperatures (from 1040 to 1180 °C) [13,20] using quasi-static (< 1 s^{-1}) [14,17,18] or low strain rates (<10 s^{-1}) [13,20], failing to cover the full spectrum. As a result, they are not easily comparable, as they do not overlap in any testing condition range. Nor do they accurately reflect the manufacturing route of the tested material, which affects the microstructure and consequently the thermomechanical properties. These gaps limit understanding of the in-service behaviour of the material and selection of the appropriate manufacturing route for turbines, which includes machining (involving high strains, strain rates, and temperatures) and forging (low strain rates and high temperatures) to ensure component quality. Critically, significant discrepancies can also be found in the literature regarding the adiabatic heating correction methodology for thermomechanical characterisation tests in nickel-based alloys, leading to conflicting conclusions about the influence of strain, strain rate, and temperature on the thermomechanical properties. This inconsistency stems from a lack of analysis on the impact of various adiabatic heating correction methods, hindering the development of a unified approach that ensures comparability of results across studies.

This paper, therefore, characterises the thermomechanical properties of forged and heat-treated Udimet 720Li across a broad temperature and strain rate range and proposes a novel adiabatic heating correction procedure. To this end, a detailed microstructural analysis of Udimet 720Li was carried out to determine the phases that make up the material and the microstructural anisotropy produced by the forging process. A full thermophysical characterisation (specific heat, density, diffusivity, thermal expansion, and conductivity) was then conducted over a wide temperature range (20–1200 °C) to obtain input data for the adiabatic heating correction. Finally, the thermomechanical properties of Udimet 720Li were determined by performing compression tests. Temperatures (T) from room temperature (20 °C) to 1100 °C were tested, and the strain rate ($\dot{\varepsilon}$) was varied from 0.01 s^{-1} to 100 s^{-1}. The influence of different methods of adiabatic heating correction and microstructural anisotropy on the thermomechanical properties of the Udimet 720Li was also analysed.

2. Materials and methods

2.1. Material description

Udimet 720Li samples were extracted from a forged disc which was solution treated and precipitation hardened (required for intended final use). The chemical composition of Udimet 720Li reported in the literature is presented in Table 1.

Table 1
Chemical composition of Udimet 720Li in weight percent (wt. %) [3,16–20].

Al	B	C	Co	Cr	Fe	Mo	N	Ti	W	Ni
2.57	0.015	0.011	14.7	16.3	0.01	3	0.002	5.02	1.31	Bal

2.2. Microstructural characterisation

The microstructure of Udimet 720Li was characterised by optical microscopy, Scanning Electron Microscopy (SEM) and X-Ray diffraction techniques. The SEM measurements included Energy Dispersive X-Ray Spectroscopy (EDS) and Electron Backscatter Diffraction (EBSD) analysis.

Udimet 720Li samples were extracted by wire-Electro Discharge Machining (EDM) from several zones of the bulk of the forged disc, close to the inner and outer diameters, to analyse the microstructural heterogeneity. Those samples were ground, polished, and chemically etched. Initially, the average grain size was determined using the Average Grain Intercept methodology, following ASTM E112-13 standard. The equipment used to analyse the samples was a Leica DM IRM optical microscope using LAS V4.9 software. To analyse the distribution of phases in the microstructure, a SEM FEI Nova NanoSEM 450 was used with 15 kV acceleration voltage and 5.5 mm working distance. Quantitative measurements of the γ' size and volume fraction were directly obtained from SEM EDS maps using an automated image analyser integrated into the AZtec software from Oxford Instruments, similar to the procedure reported in the literature [10,35,36]. The samples for EDS and EBSD characterisation were vibropolished after polishing with 1 μm diamond suspension, rather than chemically etched. To obtain statistically reliable data, ten images were analysed in each sample extracted from different regions of the forged disc.

A more detailed analysis of the microstructure was also conducted with EBSD. An area of ≈ 50 x 50 μm^2 was mapped with a step size of 0.05 μm and an acceleration voltage of 20 kV. Then, the Kernel Average Misorientation (KAM) was calculated using AZtec software. KAM is a good indicator of the plastic strain arising from dislocations, which enables the evaluation of the microscale plastic strain produced by previous manufacturing processes [37,38].

Texture analysis of the as-received sample was performed with a Bruker D8 Discover X-Ray Diffractometer provided with a Cr-sealed tube at 40 kV and 40 mA. The diffraction data was acquired using a 1D linear position-sensitive detector. Three incomplete pole figures of {111}, {200} and {110} were measured. These pole figures were used to calculate the Orientation Distribution Function (ODF) and the complete pole figures, using the Harmonic Method.

Finally, hardness measurements were carried out on the samples prepared for optical microscope analysis using Nexus 412A equipment. A Vickers hardness test was conducted with 1 kg of load applied for 10 s. Ten tests were carried out in each zone (close to the inner and outer diameters).

2.3. Thermophysical characterisation

Obtaining the thermophysical properties for a wide range of temperatures not only allows robust correction of the adiabatic heating of thermomechanical characterisation tests (see equation (1)) but also provides insight into the phase transformations that the material undergoes at different temperatures. It is also a key parameter in finite element simulations of manufacturing processes (e.g., forging, machining), as it affects the prediction of scientific variables (forces, temperatures, etc.) and industrial outcomes (surface integrity, wear, distortions, etc.) [39,40].

The specific heat (C_p), density (ρ), diffusivity (κ), and thermal expansion (α_s) of Udimet 720Li were experimentally characterised, while the thermal conductivity (λ) was obtained analytically with equation (2), taking into account the remaining characterised variables.

$$\lambda(T) = \rho(T)\cdot C_p(T)\cdot\kappa(T) \quad (2)$$

It is well established that temperature strongly influences the thermophysical properties of a material, and thus all the thermophysical parameters in this study were characterised as a function of temperature. The influence of temperature was analysed between 20 °C and 1200 °C, except for diffusivity, where the maximum temperature was limited to 1100 °C to prevent the possible melting of the specimen in the case of overheating produced by the laser used to measure this property. All tests were carried out at a heating rate of 10 °C·min^{-1} and all the tests were done in an inert atmosphere using argon (density, thermal expansion and thermal diffusivity) or nitrogen (specific heat) to prevent oxidation of the samples.

The cylindrical samples were extracted from multiple regions of the disc by wire-EDM, and then the top and bottom faces were ground to ensure parallelism. The material was sourced from the same discs and zones from which the microstructural characterisation samples were obtained. Three repetitions were done for each of the analysed properties.

Details about the specimen geometry and equipment used in the thermophysical characterisation are provided in Section 1 of the Supplementary data.

2.4. Thermomechanical characterisation

Uniaxial compression loading of the Udimet 720Li specimens was accomplished using a Gleeble 3500 thermomechanical testing machine (see Fig. S1) for a wide range of temperatures (20–1100 °C) and strain rates (0.01–100 s^{-1}). Cylindrical specimens with dimensions Ø6 x 9 mm were used in the compression tests in accordance with the ASTM E9-09 and ASTM E209-00 (2010) standards. These Udimet 720Li specimens were obtained by wire-EDM from the same zones of the forged discs used for microstructural and thermophysical characterisation. Then, the flat faces of the specimens were ground to ensure parallelism and good contact with the anvils during the compression tests.

The microstructural analysis revealed heterogeneity in the Udimet 720Li samples (small grains in a preferential direction), although no texture was observed (these results are discussed in detail in Section 3.1). For this reason, complementary compression tests were conducted to determine if microstructural heterogeneity affects the isotropic behaviour of the material. To this end, specimens were manufactured in the three directions: forging direction (parallel to the thickness of the forged disc) and in the two other orthogonal directions with respect to the forging direction. Compression tests were carried out at three temperatures (20, 600, and 900 °C) and at a constant strain rate (1 s^{-1}) for specimens extracted in each direction.

Section 2 of the Supplementary data provides detailed information on the experimental procedure followed during the thermomechanical characterisation tests.

2.5. Adiabatic heating correction

The stress–strain (σ-ε) curves must be corrected since adiabatic heating occurs during tests. Two methodologies were analysed to calculate the temperature rise produced by the adiabatic heating (ΔT_{adb}). On the one hand, the analytical equation (1) (explained in Section 1) was used. The values of ρ and C_p for each temperature were taken from the thermophysical characterisation tests described in Subsection 2.3. The selected value of β was 0.9 based on the literature [29], as it is the most widely used value, even though there are significant discrepancies between studies as mentioned in the introduction. The η_{adb} was selected based on the tested strain rate following the recommendations reported in the literature [34]. The comparison between adiabatic heating correction methods is not affected by the selection of this parameter, as they are not used in the thermal balance analysis equations (equations (3) and (4)) employed for this comparison. On the other hand, the temperature rise was directly measured with the thermocouple.

Then, after calculating the temperature rise, the theoretical isothermal flow stress curves were obtained from the measured values applying the first-order Taylor Series Expansion [41]. Fig. S2a illustrates the Taylor Series Expansion approach, and a hypothetical example is presented in Fig. S2b. Finally, the yield stress (σ_y) and ultimate strength (σ_u) were extracted from the corrected curves.

To select the methodology to correct adiabatic heating more representative of the real situation, a thermal analysis was carried out. The power losses generated by radiation ($\dot{Q}_r$) were calculated by the Stefan-Boltzmann equation (3) and compared with the power generated by deformation ($\dot{Q}_d$) calculated with equation (4). This enabled analysis of the balance between the heat generated by the deformation and the heat lost during the test, which is linked to the temperature rise of the sample.

$$\dot{Q}_r = A_r \varepsilon_e \sigma_{SB} \left(T_{sur}^4 - T_{air}^4\right) \tag{3}$$

$$\dot{Q}_d = A_r L_0 \int_0^{\varepsilon_f} \sigma \mathrm{d}\varepsilon \tag{4}$$

where, A_r is the section of losses (external area of the specimen), ε_e is the effective emissivity, σ_{SB} is Stefan-Boltzmann's constant (5.67·10^{-8} W·m^{-2}·K^{-4}), L_0 is the initial length of the specimen, ε_f is the strain to fracture, and T_{sur} and T_{air} are the surface and ambient temperatures, respectively, measured with the thermocouple.

The only variable that needed to be characterised was the effective emissivity, which was determined by measuring the surface temperature of a flat specimen with the thermocouple and an infrared camera (FLIR Titanium 550 M). The calibration was carried out at room temperature to prevent possible sample oxidation, as the vacuum needs to be removed to enable filming. The effective emissivity was obtained with the diffuser reflector method, which is commonly employed to determine this temperature, as it is easy to apply and provides robust results [28,42]. The reflector is placed in the field-of-view, far from the heat source, and its temperature is measured taking into consideration an emissivity of one and a distance of zero (apparent temperature). As the material was self-heated during the test due to the adiabatic heating phenomenon, this self-heating was employed as the heat source, and the apparent temperature of the anvil was used to determine the reflected temperature. Based on this analysis and previous research by the authors [28], the reflected temperature was set to 32 °C. A 3 × 3 pixel was put close to the thermocouple to calculate the emissivity, which was measured as 0.71. This was considered constant with temperature as the samples were in a vacuum, which prevents oxidation.

3. Results and discussion

3.1. Initial microstructure

Fig. 1a and b show the micrographs of the forged disc of Udimet 720Li close to the inner (internal) and outer (external) diameters obtained with the optical microscope. Both regions showed almost identical microstructure. Nevertheless, considerable heterogeneity in grain size can be observed inside each zone.

The large and small grain size zones inside the external and internal

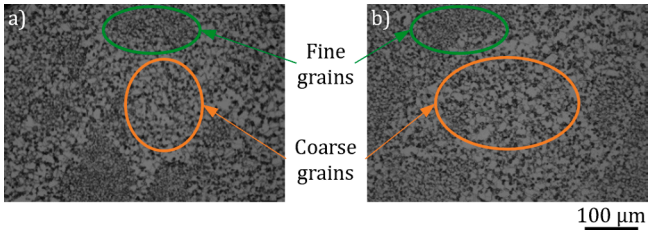

Fig. 1. Optical micrographs of Udimet 720Li extracted from the a) external, and b) internal zones of the disc.

regions were measured in detail to obtain two grain size values to quantify the heterogeneity. The grain size number (G) for the coarse grain in the interior and exterior zones was $G = 8.8 \pm 0.2$ and $G = 8.6 \pm 0.2$, respectively, while the fine grain was $G = 10.4 \pm 0.2$ and $G = 11.0 \pm 0.2$, respectively. These measurements confirmed that there were no significant differences in grain size between the internal and external zones of the forged disc, but within each region a heterogenous microstructure was found with a mixture of coarse and small grains. This observation is in agreement with [13,17,18], who measured grains between $G = 10$ (≈ 11 μm) and $G = 8$ (≈ 22 μm) in Udimet 720Li.

The hardness was measured in the fine and coarse grain size zones (see Fig. S3). The indentation size was $\approx 65 \times 65$ μm, and as a result it was difficult to ensure that each indentation only tested fine grains or coarse grains. However, the indentations were able to statistically test sufficient grains from each zone, as can be seen in Fig. S3a (fine grains) and in Fig. S3b (coarse grains), to assess the differences in hardness. The average hardness in the fine grain size zone was 450 ± 7 HV_1, slightly higher than in the coarse zone (439 ± 8 HV_1). As expected from the Hall-Petch effect, a reduction in grain size leads to an increase in hardness [43]. Nevertheless, the difference is within the measurement uncertainty, and therefore, the effect of grain heterogeneity on hardness is negligible.

Subsequently, a phase analysis was carried out with the SEM. Fig. 2 shows the Secondary Electron (SE) micrograph of the Udimet 720Li using different magnifications. The micrograph clearly reveals the presence of primary γ' precipitates in the grain boundaries of the γ matrix phase. The primary γ' is one of the main strengthening phases of the material [44–46], and is the γ' which remains undissolved during the solution treatment when the temperature is below the $\gamma/(\gamma + \gamma')$ solvus [46]. It forms through the precipitation hardening of $Ni_3(Al, Ti)$ particles and M(C, N) (carbon nitride precipitates) at the γ grain boundaries. The primary γ' precipitates exhibit an irregular shape, with sizes ranging from 2 to 10 μm and an average size of 5 μm. The volume fraction is approximately 30 %, consistent with values reported in the literature [11,35,46].

At higher magnification, the presence of secondary γ' was observed inside the γ phase, contributing to the hardening effect. This phase is highly dependent on the cooling rate of the solutioning temperature [46]. Secondary γ' precipitates are spherical shape with sizes ranging from 60 to 100 nm, averaging 80 nm. The size and shape of both primary and secondary γ' precipitates align with those reported for forged and heat-treated Udimet 720Li microstructures in the literature [46,47]. The detrimental phase sigma composed of CrNi [44,46] was not observed.

EDS analysis was conducted to achieve a more in-depth analysis of the chemical composition of the phases detected in the general overview of the microstructure. A map analysis was carried out to more precisely determine the location of the primary γ' and γ phases (see Fig. 3), confirming that the main elements present in γ' are aluminium, titanium, and nickel. Some examples of each phase are illustrated in Fig. 3.

A point analysis was conducted in each phase to more precisely identify the chemical composition of the phases, although this type of analysis provides qualitative results. The points of analysis are identified in Fig. 3. P1 is primarily located in the γ phase, and P2 in the γ'. Table 2 shows the measured chemical composition of each point. The chemical composition of the γ phase was similar to the overall composition of the Udimet 720Li reported in the literature [3,16–20] and is set out in

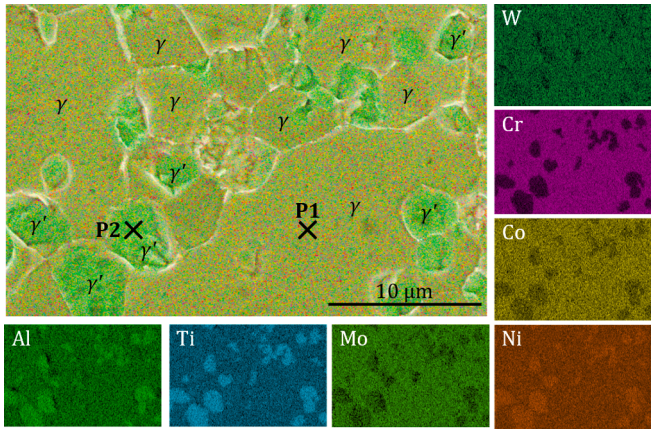

Fig. 3. Map of the chemical composition of Udimet 720Li.

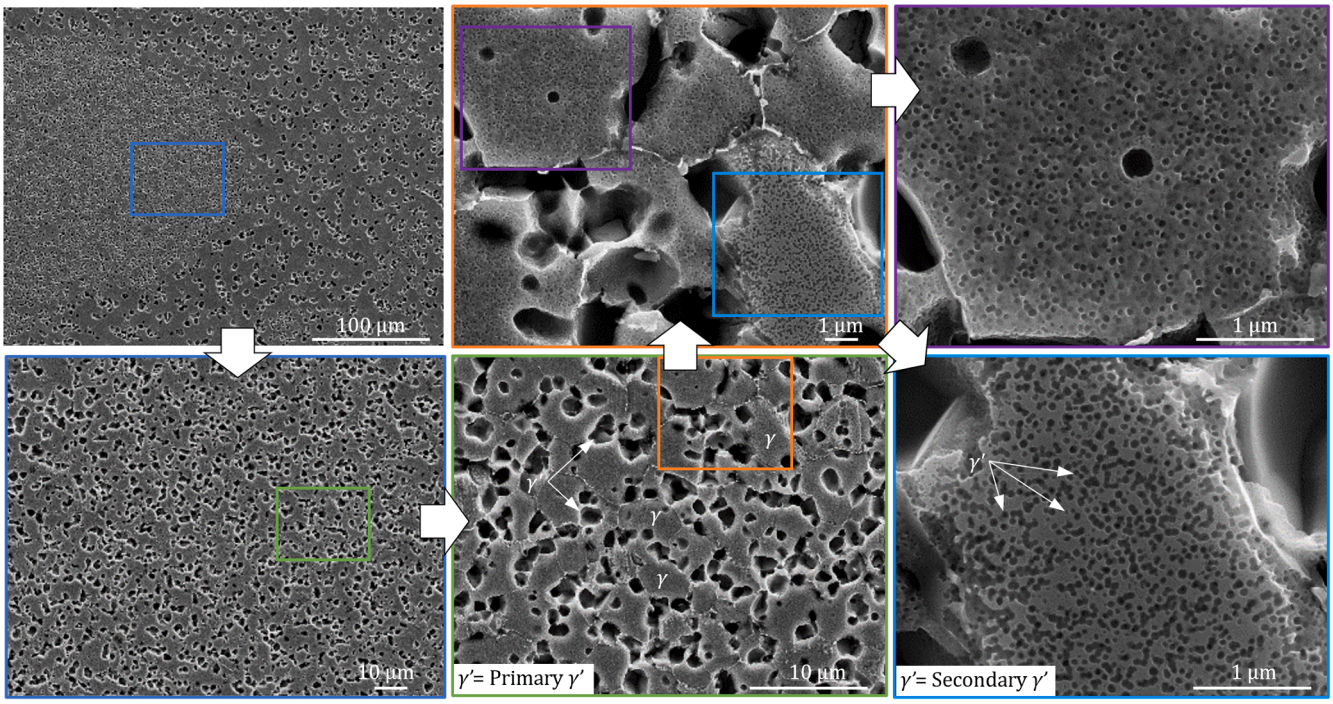

Fig. 2. SE micrograph of Udimet 720Li measured with the SEM at various magnifications.

Table 2
Chemical point analysis results of the Udimet 720Li.

Point		Al	Co	Cr	Mo	Ti	W	N	Ni
P1 (γ)	% Weight	2.1	15.8	18.9	3.5	3.9	1.7	–	54
	%Mole	4.4	15.3	20.8	2.1	4.6	0.5	–	53.2
P2 (γ')	% Weight	4.5	8.8	3.7	0.6	11.4	0.9	–	70.2
	%Mole	9	8.2	3.9	0.4	13	0.3	–	65.3
P3 (TiN)	% Weight	–	–	–	–	77.5	–	20.6	–
	%Mole	–	–	–	–	52.4	–	47.7	–

Table 1. The γ' phase presented significantly higher titanium, nickel, and aluminium content than the matrix γ. The composition of the γ' phase was determined by calculating the mole fraction (see Table 2), resulting in Ni_3(Al, Ti) as reported by other authors [44,46].

Other particles observed in the microstructure were also analysed. The chemical composition map showed that the main elements of the particle were titanium and nitrogen (see Fig. 4). In the boundaries of the particle, carbon and tungsten content were significantly higher than in the γ phase. A subsequent point analysis of the composition of the particle (P3 marked in Fig. 4) confirmed that the main elements present in the particle were nitrogen and titanium (see Table 2). The mole fraction indicated that there was a mole of nitrogen per mole of titanium, and therefore these particles are TiN. These particles were also found by other researchers in nickel-based alloys [20,44].

An EBSD analysis was then carried out to analyse the initial misorientation of the grains produced by previous manufacturing processes: forging and heat treatment (solution treated and precipitation hardened). Fig. 5a and b show the Euler angles and Inverse Pole Figures (IPF) maps, respectively. No evidence of preferential direction of the crystallographic orientation can be observed. Additional measurements were carried out in several areas with both fine and coarse grains, confirming the absence of preferential direction. Twining phenomena commonly reported in nickel-based alloys can be observed in this map. This is linked to the forging process (some examples are marked in Fig. 5a), as also observed in the literature for Inconel 718 [48].

Fig. 5c shows the Kernel Average Misorientation (KAM). In general, the highest misorientations were located in the vicinities of twins, and the maximum misorientation values observed were ≈ 1°. These misorientation levels are relatively low compared to processes involving severe plastic deformation, such as machining, where KAM can exceed

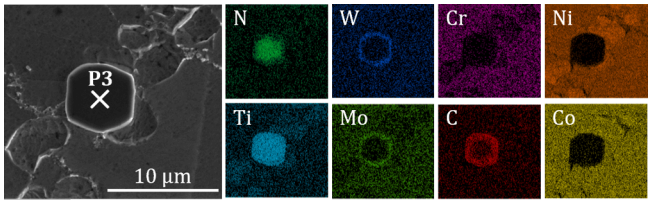

Fig. 4. Chemical composition of a TiN precipitate.

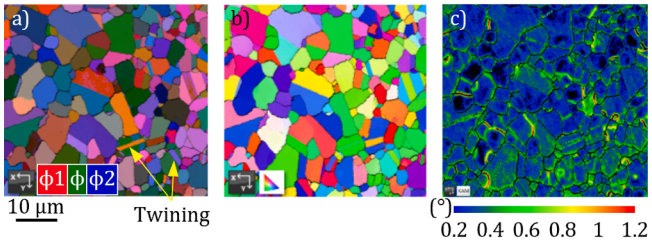

Fig. 5. EBSD measurements of Udimet 720Li: a) Euler angles, b) IPF, and c) KAM (all at the same scale) maps.

3° near the machined surface [38], or forging, where KAM values can reach up to 4° [37]. Although forging induces plastic deformation and therefore high dislocation density, the subsequent heat treatments have reallocated the dislocations, leading to lower KAM values [37].

Finally, the microstructure was observed in three directions (see Fig. 6a) to determine whether the accumulation of fine/coarse grains was homogeneous in all three or exhibited a preferential direction. A preferential direction could produce the anisotropic behaviour of the material. The figure shows fine grains accumulating in the form of strips along the *Z*-axis, which is the forging direction, as also reported by [49]. Looking from the top the heterogeneous microstructure previously shown in the grain size analysis is observed (plane XZ).

The complete pole figures in the as-received specimen characterised by X-Ray diffraction are shown in Fig. 6b. Although the morphology of the grains is different in the three directions, these pole figures clearly show that the material was not textured since the texture index is around one. Even if different crystallographic orientations are present, as it is a polycrystalline material, they are not aligned in a preferential direction. The anisotropy of a polycrystalline material is highly dependent on the preferred orientations of the single crystals (constituting the material). In the case of an isotropic texture where all the orientations occur randomly, the behaviour of the polycrystalline material is isotropic.

3.2. *Thermophysical properties*

Fig. 7a-e show the characterised thermophysical properties of Udimet 720Li. It should be noted that the uncertainty is represented in two ways: i) error bars for results measured at fewer temperature increments (density and diffusivity) and ii) shadow for results with a large amount of data obtained in small temperature increments (specific heat, thermal expansion, and thermal conductivity). To further analyse the changes in thermophysical properties, a complementary phase analysis (γ, γ', σ) was conducted using JMatPro® software. Fig. 7f presents the phase diagram obtained using JMatPro® software, showing similar results to the literature [44] that were obtained using THERMOCAL software and Rolls-Royce thermodynamic dataset [50].

The density (ρ) decreased continuously from 8086 ± 10 kg·m^{-3} to 7581 ± 20 kg·m^{-3} (reduction of 6.2 %) when the temperature increased. The thermal expansion (α_s) increased drastically from room temperature to ≈ 150 °C. Above this temperature, it increased linearly in two regions: i) with a low slope up to ≈ 760 °C and ii) with a higher slope at the highest temperatures. This change of trends at 760 °C is related to the beginning of the dissolution of the γ' phase (see Fig. 7f), as was also observed in Inconel 718 [51].

The specific heat (C_p) maintains a constant value up to 550 °C, between 460 to 480 J·kg^{-1}·°C^{-1}. Above this temperature, abrupt results are observed at different temperatures (600, 760, 900, and 1150 °C). Specific heat not only depends on the intrinsic ability of a material to absorb energy but also on the energy absorption/release during microstructural phase changes [52]. Consequently, when the material undergoes phase changes, the specific heat deviates from the smooth curve, as observed in Fig. 7c for Udimet 720Li. Thus, the multiple variations in C_p are related to the phase transformations of the material. In the phase diagram of Fig. 7f, it can be seen that the sudden increase of the C_p at 760 °C seems to be caused by the beginning of the dissolution of the γ' and σ phases, although the σ phase was not detected in the microstructural analysis. Subsequently, a trend change is observed at approximately 900 °C due to the completion of the σ phase dissolution. From this temperature onwards, drastic changes in C_p continue to occur, becoming more abrupt as the dissolution of the γ' phase with temperature becomes more significant (above 1000 °C). Similar trends were observed for Inconel 718 [51], but at lower temperatures than Udimet 720Li, as it has a lower strengthening phase content, and its dissolution starts at lower temperatures [9].

Diffusivity (κ) was also significantly affected by the abrupt dissolution of the γ' phase (see Fig. 7f) above 1000 °C. Diffusivity increased

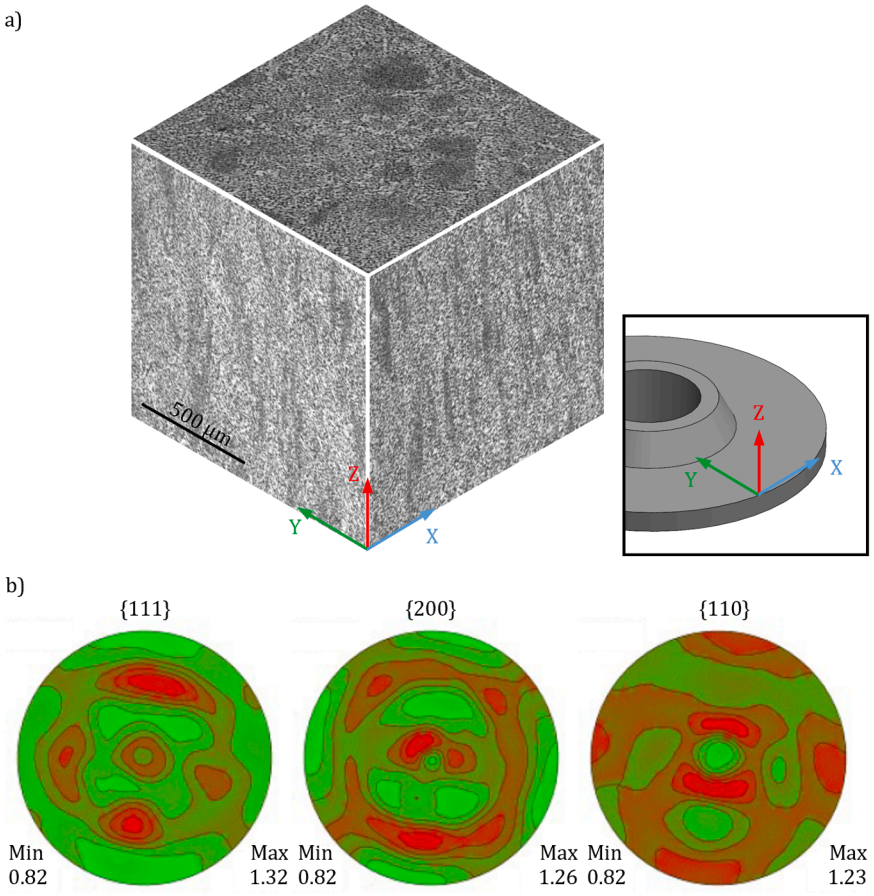

Fig. 6. a) 3D microstructure and b) {111}, {200} and {110} pole figures of Udimet 720Li.

linearly up to 1000 °C, and started decreasing above this point. This change in the evolution of κ with respect to temperature was also observed in Inconel 718 but at lower temperatures (≈ 900 °C) [51] than Udimet 720Li for the same reasons as those of the C_p.

Once all the thermophysical properties were characterised, the thermal conductivity (λ) was calculated using equation (2). As the results are a combination of previously analysed thermophysical properties, the results present a similar trend: a linear increase from 12 ± 0.2 $W{\cdot}m^{-1}{\cdot}°C^{-1}$ at 20 °C up to 20.4 ± 0.3 $W{\cdot}m^{-1}{\cdot}°C^{-1}$ at 760 °C, then abrupt changes in the thermal conductivity at 760, 1000, and 1100 °C which are related to the phase changes (see Fig. 7f) already discussed.

To demonstrate that changes in thermophysical properties are due to phase changes and to highlight the importance of obtaining properties from materials produced under industrial conditions, an additional test was conducted using a specimen composed solely of the γ phase. For this purpose, a specimen was pre-heated to 1200 °C to completely dissolve the γ' phase. The detailed results and discussion of this test are provided in Section 6 of the Supplementary data. It was observed that the C_p values (see Fig. S4) were markedly different from those observed in the forged and heat-treated Udimet 720Li shown in Fig. 7c. This underscores the need to characterise the thermophysical properties of the material based on the specific manufacturing process for a given application, as alterations in the thermal history can result in significant variations in properties. These variations can affect adiabatic heating corrections or the accuracy of thermal field predictions in a wide range of finite element simulations, including high-temperature structural analysis, heat transfer studies, as well as various manufacturing processes (forging, machining, welding, heat-treatment, etc.).

3.3. Influence of adiabatic heating

To propose a new methodology for correcting adiabatic heating, the temperature increase caused by thermomechanical tests was determined using two approaches: i) analytically with equation (1), and ii) experimentally using temperature measurements from a thermocouple. This comparison was further assessed through an energy balance study. Fig. 8a shows examples of the temperature rise obtained from both methods for selected tested temperatures at multiple strains (ε). As can be observed, the analytical equation always shows a higher temperature increase than the thermocouple measurements. Up to 600 °C both techniques present an incremental rise in temperature with deformation, although with a different slope. Above this temperature, the analytical equation always depicts a linear increase, while the thermocouple shows a reduction in the temperature above ≈ 0.4 strain.

The difference between the two methodologies did not produce significant changes in the corrected flow stress at low temperatures (see Fig. 8b). This is mainly because the influence of temperature on flow stress is quite low up to temperatures of 600–800 °C. Consequently, the variation in flow stress is negligible when the isothermal correction is applied. Nonetheless, for materials such as steels [53] or aluminium alloys [54], where temperature significantly affects flow stress at lower temperatures, accurately selecting the adiabatic heating correction method may be crucial even at low temperatures. As shown in Fig. 8a, discrepancies in the quantification of temperature rise between both methods are evident at low temperatures.

However, at higher temperatures in Udimet 720Li, where small temperature changes significantly reduce the flow stress, the results can differ considerably depending on the selected adiabatic heating correction methodology. This was particularly evident at high strains

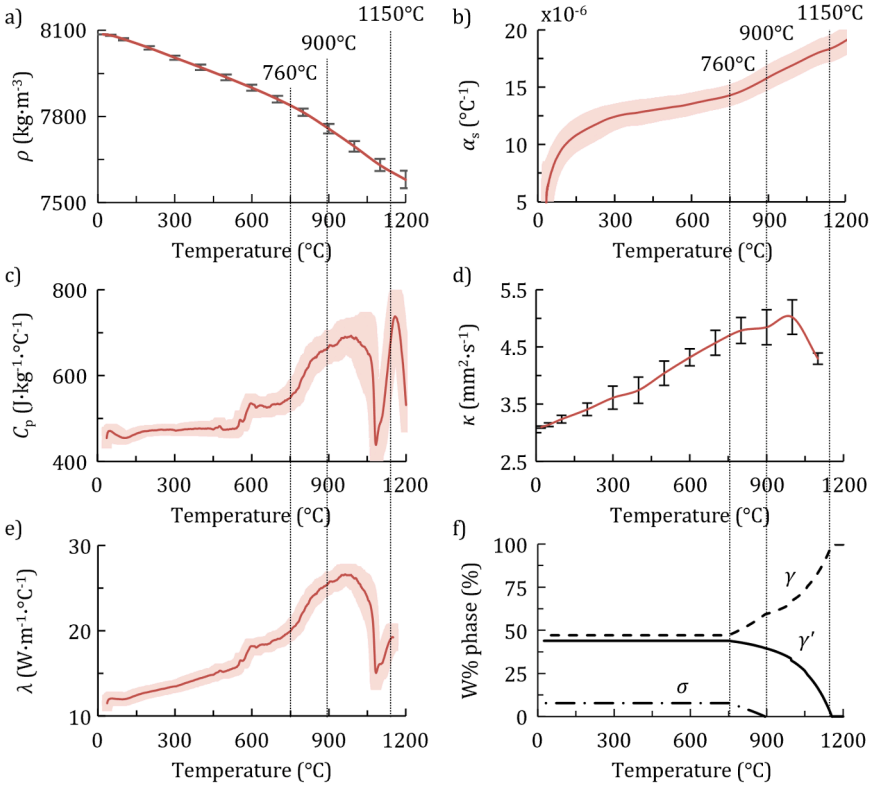

Fig. 7. Evolution of a) density (ρ), b) thermal expansion (α_s), c) specific heat (C_p), d) diffusivity (κ), and e) thermal conductivity (λ) as a function of temperature. f) Phase diagram obtained using JMatPro®.

where the differences in flow stress corrected by the analytically calculated temperature rise, and the experimental temperature were the highest (see Fig. 8a). For instance, at 900 °C using the analytical equation to calculate the temperature increase, the flow stress shows a slight strain softening followed by an unexpected hardening at strains above ≈ 0.6. In the case of the thermocouple, an evident strain softening is observed for strains greater than ≈ 0.3 (see Fig. 8b).

The differences in experimentally measured and analytically calculated adiabatic heating are mainly the consequence of the effect of heat losses. To understand the relevancy of heat losses to testing temperature and strain rate, an energy balance was carried out (see Fig. 9). The figure shows the power losses generated by radiation ($\dot{Q}_r$) in the left axis and in the right axis the power of the deformation ($\dot{Q}_d$) calculated by equations (3) and (4) respectively (procedure explained in Subsection 2.5) for all the tested temperatures and strain rates. It should be noted that for strain

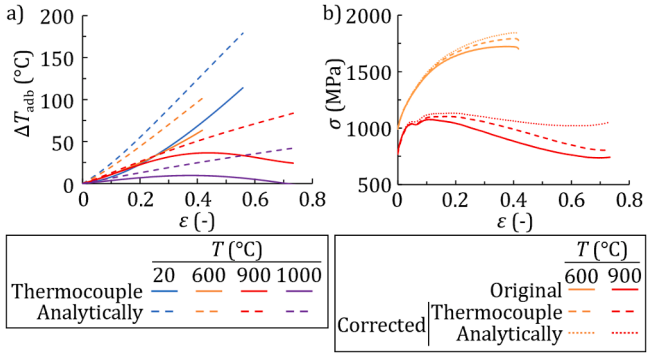

Fig. 8. a) ΔT_{adb} calculated analytically and from the thermocouples, and b) original and corrected flow stress curves using the ΔT_{adb} obtained with the analytical equation and the thermocouples for 600 and 900 °C (all tests at $\dot{\varepsilon} = 1\ s^{-1}$).

rates of 100 s^{-1}, only the deformation power is presented. This is because in such fast tests the thermocouple cannot accurately measure the temperature increase. Furthermore, it was difficult to ensure that the thermocouple was not detached during deformation, potentially giving rise to erroneous values.

As the temperature increased up to 760 °C at strain rate of 1 s^{-1}, the deformation power $\dot{Q}_d$ decreased due to its dependence on stress and strain. This decrease is attributed to the reduction in thermomechanical properties caused by thermal softening (explained in detail in Subsection 3.4). $\dot{Q}_d$ then rose sharply between 760 and 800 °C before continuing to decrease beyond this range. Within 760–800 °C range, a significant increase in specific heat was observed (see Fig. 7c), corresponding to the start of the dissolution of the γ' phase, as analysed in the thermophysical characterisation tests (see Fig. 7f). The dissolution of this phase not only reduced thermomechanical properties but also enhanced ductility by diminishing the precipitation hardening effect, significantly increasing the strain to fracture from 0.3 at 760 °C to 0.7 at 800 °C. Therefore, despite the reduction in thermomechanical properties, the $\dot{Q}_d$ increased. Finally, above 900 °C, $\dot{Q}_d$ decreased sharply due to a more rapid dissolution of the γ' phase with increasing temperature (see Fig. 7f), which significantly affected the thermomechanical properties (explained in detail in Subsection 3.4) without markedly impacting ductility.

As the strain rate increased, the $\dot{Q}_d$ followed the same trend, with the only difference being the temperature at which it began to drop sharply. At $\dot{\varepsilon} = 1\ s^{-1}$, this reduction started at 900 °C, while at $\dot{\varepsilon} = 100\ s^{-1}$, it occurred at 1000 °C. This is because strain rate hardening generates more $\dot{Q}_d$ due to the increase in the thermomechanical properties even though these are significantly reduced by the severe dissolution of the γ' phase—leading to a decrease in $\dot{Q}_d$. Additionally, a coupling between temperature and strain rate was observed (explained in Subsection 3.4), meaning that as the temperature rises, strain rate hardening intensifies, causing the sharp reduction in $\dot{Q}_d$ to occur at higher temperatures with

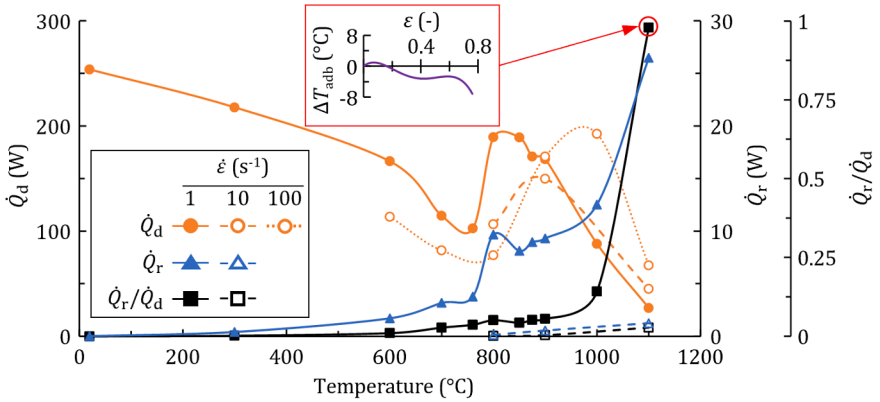

Fig. 9. Deformation power ($\dot{Q}_d$), radiation power ($\dot{Q}_r$), and the ratio between them ($\dot{Q}_r/\dot{Q}_d$) which includes an inset at $\dot{\varepsilon} = 1\ s^{-1}$ and $T = 1100\ °C$.

increasing strain rates.

$\dot{Q}_r$ increased with temperature, with the most drastic increase occurring above 900 °C. This is because the higher the difference between the temperature of the surface of the specimen and the room temperature, the greater the losses (see equation (3)). Additionally, at $\dot{\varepsilon} = 10\ s^{-1}$ the radiation losses were small in comparison to $\dot{\varepsilon} = 1\ s^{-1}$, due to the shorter test time. For instance, at 800 °C and $\dot{\varepsilon} = 10\ s^{-1}$ $\dot{Q}_r = 0.15$ W, which is lower than the radiation losses at $\dot{\varepsilon} = 1\ s^{-1}$ and 300 °C ($\dot{Q}_r = 0.42$ W). Hence, the assumption made that at $\dot{\varepsilon} = 100\ s^{-1}$ there is no significant radiation losses is correct, which indicates that the analytical equation is correct for this condition.

Finally, the ratio between the radiation losses and the power generated by the deformation ($\dot{Q}_r/\dot{Q}_d$) is plotted on the right-hand secondary axis of Fig. 9. At $\dot{\varepsilon} = 1\ s^{-1}$ and temperatures below 600 °C, the influence of radiation loss is insignificant (below 1 %). However, as the temperature rises, radiation losses play a more fundamental role, until at 1100 °C they are equal to those generated by the deformation. Therefore, at 1100 °C and $\dot{\varepsilon} = 1\ s^{-1}$ the temperature slightly increases at the beginning of the deformation produced in the strain hardening region (see the small inset graph with red borders in Fig. 9). In contrast, at $\varepsilon > 0.2$ the temperature decreases despite the deformation heating due to the high radiation losses. A similar phenomenon can be observed in Fig. 8a for $\dot{\varepsilon} = 1\ s^{-1}$ and 1000 °C, where the temperature decreases at $\varepsilon > 0.4$ owing to the substantial radiation losses (14 %).

It is thus evident that when testing at high temperatures and low strain rates (specially below 1 s^{-1}), radiation losses need to be considered to calculate adiabatic heating. Nonetheless, in other materials where the properties diminish at lower temperatures (e.g., steels, aluminium [53,54]), radiation losses may need to be considered even at low temperatures, as they can impact the corrected flow stress curve. As the strain rate increases, however, the importance of radiation losses decreases sharply, and can even be disregarded. Hence, based on the present results, the use of the analytical equation for adiabatic heating correction at high strain rates (100 s^{-1}), and thermocouple measurements for low strain rates (1 and 10 s^{-1}) is justified for Udimet 720Li and likely applicable for other nickel-based alloys and materials.

3.4. Thermomechanical properties

The microstructural analysis reveals that the primary γ' phase accumulates in a preferential direction (see Fig. 6). However, the pole figures did not indicate any texture, suggesting isotropic behaviour of the material. To determine whether the grain size affects thermomechanical properties, compression tests were carried out on specimens obtained in three microstructural orientations, at three temperatures (20, 600, and 900 °C) and a constant strain rate of 1 s^{-1}. Based on the adiabatic heating correction analysis, the thermocouple values were used to correct the adiabatic heating of the tests carried out at strain rates below 10 s^{-1} and the analytical equation for 100 s^{-1}.

Fig. S5 shows the orientation of the specimens as extracted from the forged disc and identifies the orientation of the stripes composed of fine grains (represented in dashed lines). The compression test results of the isotropic analysis are also set out in the figure. The samples with the strips of fine grains in the direction of the deformation (Z axis) present a slightly higher yield strength (<5%) than those observed in the other directions. However, once the strain increases above ≈ 0.1, the flow stress curves of the specimens extracted in three directions follow the same trend, with negligible differences (<2%). These values are within the uncertainty of the measurements. It can thus be concluded that the material behaves isotropically even though fine grains are elongated in the Z direction.

Having confirmed that the morphology of fine grains does not affect the isotropic behaviour of Udimet 720Li, a complete thermomechanical characterisation was conducted employing specimens with fine grains aligned in the Z direction (forging direction). More than 100 tests were carried out, varying the temperatures from 20 to 1100 °C and the strain rate from 0.01 to 100 s^{-1}. Fig. 10 shows the evolution of yield stress (σ_y) and ultimate strength (σ_u) with respect to temperature and strain rate for Udimet 720Li after applying the adiabatic heating correction procedure. A single temperature (20 °C) was tested for a strain rate of 0.01 s^{-1}. These results are not included in the graph as the value overlapped those of 1 s^{-1}. The figure also includes the values obtained by Iturbe et al. [9] and Devaux et al. [19] for Inconel 718, as this is the most widely used nickel-based alloy in critical aeroengine components [6]. The right axis of the figure shows the weight percentage evolution of the hardening phase γ' with respect to temperature for both alloys. This was calculated with JMatPro®. Although there may be variations between the software database and the material employed in this research, the evolution of γ' phase content with temperature from the software matches the values reported in the literature [9,13,14,44] and those measured in this study for Udimet 720Li at room temperature (presented in Subsection 3.1). It can therefore be assumed that the software can provide appropriate qualitative information.

At a 1 s^{-1} strain rate, a slight linear decrease in Udimet 720Li properties was observed up to ≈ 760 °C. This was due to the thermal activation with increasing temperature, which produced softening [55]. As the temperature increases, the energy available to overcome barriers to dislocation movements also increases, signifying that less applied stress is required to generate plastic strain, leading to lower yield strength and ultimate strength. This is also supported by the Arrhenius equation, which can be used to relate the reduction in yield stress to the activation energy and temperature rise [25].

From 760 °C onwards, a sudden decrease of properties was observed. For instance, from room temperature to 800 °C, the yield stress dropped by only ≈ 20 %, while an increase in temperature from 800 °C to 1000 °C produced a reduction of 60 % with respect to yield stress at

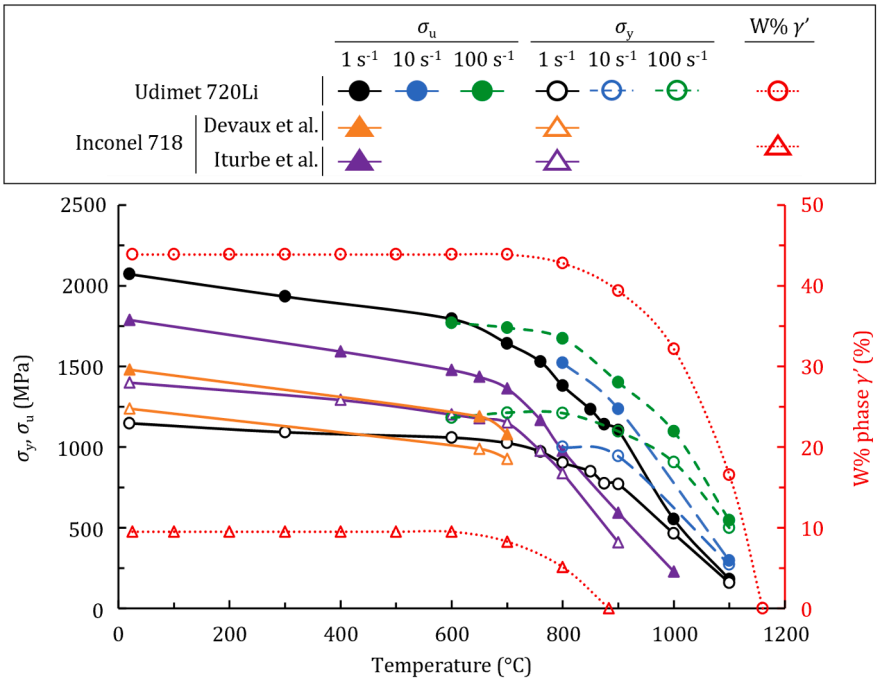

Fig. 10. Effect of temperature and strain rate on yield stress (σ_y) and ultimate strength (σ_u) of Udimet 720Li and Inconel 718. Inconel 718 results are from Iturbe et al. [9] and Devaux et al. [19]. Includes the evolution of γ' phase with temperature from JMatPro®.

room temperature. Similar behaviour was also observed in the ultimate strength. This drastic reduction in thermomechanical properties is primarily associated with the dissolution of the γ' phase (see the right axis of Fig. 10) which reduced the precipitation hardening effect. The higher the temperature, the greater the dissolution phenomena, leading to a more significant reduction in thermomechanical properties.

As regards the influence of the strain rate, it was observed that increasing the strain rate had minimal impact on material properties at low temperatures. In contrast, at high temperatures it induced a hardening effect, as expected, due to increased dislocation density and dislocation pileup [56,57]. This insensitivity to strain rate at low temperature has been previously reported in the literature; when conducting tensile tests of Udimet 720Li no strain rate hardening was observed at room temperature and 400 °C, but it was evident at 750 °C [17]. A similar trend—where strain rate has little effect below a threshold temperature and hardening above it—was also reported for Inconel 718 [9], steels [53], and aluminium alloys [54]. Nonetheless, the temperatures at which these transitions occur vary due to the differences in thermal stability and structure of the phases of each material.

Using a 1 s^{-1} strain rate the temperature had a limited effect on yield and ultimate strength up to ≈ 760 °C, but this threshold temperature increased to ≈ 900 °C when testing at a 100 s^{-1} (see Fig. 10). This difference in the threshold temperature at which the influence of the temperature becomes evident is because deformation always involves a competition between strain rate hardening and thermal softening related to diffusion at high temperatures. If the strain rate is high, the time available for diffusion phenomena is shorter [17]. Therefore, the thermal softening at a given temperature is reduced, and higher temperatures (with higher diffusion rates) may be necessary to observe this softening. For this reason, the drop in properties occurs at higher temperatures as the strain rate increases.

Finally, the thermomechanical behaviour of Udimet 720Li was compared to Inconel 718 (as reference) and other nickel-based alloys used in aeronautic industry. Compared to the heat-treated Inconel 718 results from Iturbe et al. [9], Udimet 720Li exhibits a 22 % lower yield stress at 1 s^{-1} and room temperature. However, above ≈ 760 °C, the Udimet 720Li presents improved properties, which are more pronounced as the temperature rises. For instance, at 800 °C, Udimet 720Li shows 7 % higher yield stress than Inconel 718, increasing to 47 % at 900 °C. It should be noted that the work of Iturbe et al. [9] did not specify whether the samples were forged, and no adiabatic heating correction was applied, which may affect these conclusions.

The results of the present work were therefore compared with those obtained for forged and heat-treated Inconel 718 by Devaux et al. [19] to extend the comparison with other studies and validate the conclusions. It should be noted, however, that the comparison is not under identical conditions, as the strain rate of Devaux et al. [19] is unknown, the tested temperature range is limited, and it is unclear whether an adiabatic heating correction was applied. In this second case, Udimet 720Li reported only an 8 % lower yield strength than Inconel 718 at room temperature, and a higher yield strength above 450 °C, with the difference reaching up to 10 % at the maximum temperature (700 °C) tested by Devaux et al. [19].

The exact temperature at which Udimet 720Li surpasses the yield strength of Inconel 718 is difficult to determine, since the values can range between 450–700 °C depending on the study [9,19]. Since both the studies under comparison applied the same heat treatment (solution heat treated at 980 °C, followed by a double state ageing at 720 and 620 °C), the observed variations stem from differences in the manufacturing route of the Inconel 718 (not forged [9], and forged [19]) and adiabatic heating corrections. This underscores the importance of using the same processing route for specimen preparation, which needs to be representative of industrial conditions, and applying a standardised testing procedure—including adiabatic heating correction—to ensure comparability of results.

Therefore, it can be seen that Udimet 720Li has a lower yield strength than Inconel 718 at room temperature but exhibits superior performance at higher temperatures. This is consistent with the observations of Beardmore [15], who determined that a lower γ' content provides improved yield strength at low temperatures but maintains these properties at lower temperatures than alloys with higher γ' content. At low γ' volume fraction and temperatures, the γ matrix is strengthened significantly by the presence of a fine γ' precipitate, whereas at higher temperatures, the γ matrix becomes a single-phase

material with low strength [15,16]. In contrast, an increased γ' phase content increases the brittleness of the material due to the hardness disparity between γ' and γ [58], leading to reductions in ductility, toughness, and yield strength. As temperature increases, the yield stress anomaly becomes the dominant factor causing alloys with higher γ' content to exhibit little to no degradation in strength—or even an increase in strength at elevated temperatures—for γ' volume fractions exceeding ≈ 40 % [15,16,49]. The origin of the yield stress anomaly is governed by the formation of different types of dislocation locks (e.g., Kear-Wilsdorf and Giamei) [49]. Those dislocation locks are mediated by planar defect structures, such as antiphase boundaries (APBs) and stacking faults, in γ' phase ($L1_2$ crystal structure) [16]. The anisotropies in APB energy and elastic properties facilitate thermally activated cross-slip from {111} to {001}, which leads to a temperature-dependent hardening response [16]. However, recent research reported that the yield stress anomaly in Udimet 720Li can be influenced by the crystallographic texture of the alloy and the loading direction [49].

As for ultimate strength, Udimet 720Li shows ≈ 14–60 % higher values than Inconel 718 [9,19] for the whole range of temperatures, with the difference becoming more pronounced at elevated temperatures. At room temperature, Udimet 720Li exhibits 14 % higher ultimate strength than the Inconel 718 results from Iturbe et al. [9] and 24 % higher than the findings of Devaux et al. [19]. This difference increases at 700 °C, reaching 17 % [9] and 33 % [19] higher values. Data for higher temperatures is only provided by Iturbe et al. [9], revealing a continuous escalation in ultimate strength differences: 29 % higher at 800 °C, 46 % at 900 °C, and 59 % at 1000 °C. The higher ultimate strength of Udimet 720Li compared to Inconel 718 can be attributed to greater strain hardening, driven by a higher γ' phase content [59,60]. The higher γ' content promotes the formation of stacking faults within the γ' precipitates [61], and their interaction effectively enhances strain hardening [59,60].

It can be clearly seen in Fig. 10 that the reduction in the thermomechanical properties of both alloys is produced when the γ' phase content starts to drop. Since Inconel 718 has a lower content of γ' phase and starts to dissolve at lower temperatures, the thermomechanical properties decrease at lower temperatures than Udimet 720Li. This larger amount of strengthening phase in Udimet 720 Li also results in a more gradual degradation of properties as temperature increases. This indicates that in the event of an in-service failure where the turbine temperature exceeds the nominal value (overheating) [62–64], the impact on the behaviour of the component might be less severe.

The in-service temperature of the Udimet was also compared to other nickel-based alloys published in the literature. Despite some outliers, it is widely accepted that the yield stress and ultimate strength of heat-treated Inconel 718 at the in-service temperature of 650 °C [9] are 1000 MPa and 1300 MPa, respectively [8,19]. Interestingly, Udimet 720Li maintains those values of yield stress at ≈ 700–760 °C and ultimate strength at ≈ 800 °C. Therefore, this could facilitate an increase in the in-service temperature of the turbine by 50–150 °C, representing an 8–23 % rise over the in-service temperature of Inconel 718, thereby enhancing the global efficiency of the engine.

Similar conclusions can be drawn from comparisons with other less common nickel-based alloys. The forged RR1000 nickel-based alloy presents thermomechanical properties comparable to those of Inconel 718 at 650 °C, under both standard (σ_y = 1000 MPa and σ_u = 1400 MPa) and optimised (σ_y = 1160 MPa and σ_u = 1170 MPa) heat treatment conditions [12]. Similarly, when compared to Allvac® 718-Plus™ and Waspaloy, both of which show a yield stress of ≈ 850 MPa and ultimate strength of ≈ 1150 MPa at 704 °C [65], Udimet 720Li demonstrates superior performance with a yield stress of 1025 MPa and ultimate strength of 1640 MPa at the same temperature. It should be noted that the studies on Inconel 718, Allvac® 718Plus™, Waspaloy, and RR1000 [12,65] do not mention whether any form of adiabatic heating correction was applied, which means the results may not be directly comparable. This underscores the need for a standardised methodology for applying adiabatic heating, as proposed in the present paper.

Hence, replacing Inconel 718 with Udimet 720Li in the design of new-generation turbines would improve engine efficiency, as the latter allows operation at higher temperatures. However, the improved thermomechanical characteristics of Udimet 720Li may present challenges to key aeroengine manufacturing processes, such as forging (e.g., premature die wear, higher forces and energy consumption, higher forging temperatures that can lead to grain growth and potential loss of mechanical properties, quality issues [66]) and machining (e.g., premature tool wear, higher forces and energy consumption, difficulty in achieving surface integrity requirements [67]). Hence, future research should focus on optimising key manufacturing processes not only through experimental methods but also by employing simulation using the material properties presented in this article.

4. Summary and conclusions

This study has investigated the nickel-based alloy Udimet 720Li as a potential substitute for the widely employed Inconel 718 in the production of critical aeroengine components. An experimental analysis of the microstructural, thermophysical, and thermomechanical characteristics of Udimet 720Li was conducted. The conclusions drawn from this research are presented below:

- The microstructural characterisation showed heterogeneity, with an accumulation of γ' grains aligned in one direction (forging direction) in the form of strips. Nevertheless, X-Ray diffraction analysis did not reveal any texture of the material, and the compression tests of cylinders carried out in three orthogonal microstructural directions did not show significant variations in the thermomechanical properties (<5%). Therefore, both analyses confirmed the isotropic behaviour of forged and age-hardened Udimet 720Li, despite the alignment of fine grains in one orientation.
- The density, diffusivity, specific heat, thermal expansion, and thermal conductivity of Udimet 720Li present a linear trend below 760 °C. Above this temperature, the specific heat, diffusivity and thermal conductivity undergo abrupt modifications in the thermal properties at approximately 760, 1000, and 1100 °C. These changes are related to microstructural phase transitions, with the dissolution of the γ' phase proving particularly critical.
- When conducting compression tests at elevated temperatures and low strain rates (especially below 1 s^{-1}), it is clear that accounting for radiation losses is crucial for accurate adiabatic heating calculations. As the strain rate increases, the significance of radiation losses diminishes markedly to the point of being negligible. Hence, based on the thermal balance analysis, the use of values obtained from external sensors (e.g., thermocouple, thermographic camera, etc.) is proposed to make the adiabatic heating correction for low strain rates ($\dot{\varepsilon} \leq 10\ s^{-1}$) and the analytical equations for high strain rates ($\dot{\varepsilon} \geq 100\ s^{-1}$).
- The yield stress and ultimate strength of Udimet 720Li obtained by compression tests at a constant strain rate of 1 s^{-1} decrease linearly from 1150 MPa and 2070 MPa at 20 °C, to 1000 MPa and 1500 MPa at 760 °C. Above this temperature, a sudden decrease in properties occurs, which is related to the reduction of the strengthening γ' phase content.
- The higher γ' phase content of Udimet 720Li, compared to Inconel 718, increases its brittleness due to the disparity between the hardness of the γ' and γ phases. As a result, Udimet 720Li exhibits lower yield strength than Inconel 718 at room temperature. However, this higher γ' content allows Udimet 720Li to maintain its mechanical properties at higher temperatures probably due to the yield stress anomaly phenomenon. In contrast, the ultimate strength is always higher in Udimet 720Li due to greater strain hardening, which is promoted by the formation of stacking faults resulting from the

elevated γ' phase content. Therefore, at all tested temperatures, Udimet 720Li presents higher ultimate strength than Inconel 718, and higher yield strength at higher temperatures (above ≈ 760 °C). The better thermomechanical properties of Udimet 720Li become increasingly evident as the temperature rises above 650–700 °C.

- Udimet 720Li shows no sensitivity to strain rate at low temperatures, while at high temperatures, its effect increases as the temperature rises. This demonstrates a coupling between strain rate and temperature. The temperature at which the transition from insensitivity to sensitivity occurs depends on the strain rate, as a higher strain rate delays diffusion. The transition for a strain rate of 1 s^{-1} occurs at ≈ 700 °C, while for a strain rate of 100 s^{-1}, it takes place at ≈ 900 °C.

It can thus be concluded that Udimet 720Li is a promising alternative to Inconel 718 in the production of more efficient aeroengine turbines. This nickel-based alloy exhibits superior thermomechanical properties at higher temperatures, representing an increase of 8–23 % in the in-service temperature of the rotor turbine disc in comparison to Inconel 718. In contrast, the increased mechanical properties at high strain rates and temperatures require higher energy to shape the material (forging and machining). Future research could therefore usefully focus on optimising the manufacturing route and designing appropriate tools to manufacture parts made with Udiment 720Li.

Declaration of competing interest

The authors declare that they have no known competing financial interests or personal relationships that could have appeared to influence the work reported in this paper.

Acknowledgements

The authors thank the TAILORSURF (PID2022-139655OB-I00), EKOPROP II (KK-2024/00102), and ERAGIN (ZE-2024/00024) projects for the financial support, as well as ITP Aero for providing the forged disc used to carry out this research. We also extend our gratitude to Cyril Fischer, Denis Soriano, Erika Dominguez, and Larraitz Azpitarte for their invaluable technical assistance in conducting the characterisation tests.

Appendix A. Supplementary data

Supplementary data to this article can be found online at https://doi.org/10.1016/j.matdes.2025.113700.

Data availability

Data will be made available on request.

References

[1] C. Bergero, G. Gosnell, D. Gielen, S. Kang, M. Bazilian, M.S.J. Davis, Pathways to net-zero emissions from aviation, Nat. Sustain. 6 (2023) 404–414.
[2] Y.J. Hu, L. Yang, H. Cui, H. Wang, C. Li, C.B.J. Tang, Strategies to mitigate carbon emissions for sustainable aviation: a critical review from a life-cycle perspective, Sustain. Prod. Consum. 33 (2022) 788–808.
[3] R.C. Reed, The superalloys: fundamentals and applications, Cambridge University Press, 2008.
[4] E. Farabi, V.V. Rielli, F. Godor, C. Gruber, A. Stanojevic, B. Oberwinkler, S. Ringer, S. Primig, Advancing structure– property homogeneity in forged Alloy 718 engine disks: a pathway towards enhanced performance, Mater. Des. 242 (2024) 112987.
[5] N. Cumpsty, Jet Propulsion: a simple guide to the aerodynamic and thermodynamic design and performance of jet engines, Cambridge University Press, 1998.
[6] R. E. Schafrik, D. D. Ward, J. R. Groh, Application of Alloy 718 in GE Aircraft Engines: Past, Present and Next Five Year, Superalloys 718, 625 and Various Derivatives (2011) 1–11.
[7] H.Y. Wan, W.K. Yang, L.Y. Wang, Z.J. Zhou, C.P. Li, G.F. Chen, L.M. Lei, G. P. Zhang, Toward qualification of additively manufactured metal parts: tensile and fatigue properties of selective laser melted Inconel 718 evaluated using miniature specimens, J. Mater. Sci. Technol. 97 (2022) 239–253.
[8] M. Švec, P. Solfronk, I. Nováková, J. Sobotka, J. Moravec, Comparison of the structure, mechanical properties and effect of heat treatment on alloy Inconel 718 produced by conventional technology and by additive layer manufacturing, Mater. 16 (2023) 5382.
[9] A. Iturbe, E. Giraud, E. Hormaetxe, A. Garay, K. Ostolaza, P.J. Arrazola, Mechanical characterization and modelling of Inconel 718 material behavior for machining process assessment, Mater. Sci. Eng. A. 682 (2017) 441–453.
[10] V.V. Rielli, E. Farabi, F. Godor, C. Gruber, A. Stanojevic, B. Oberwinkler, S. Primig, γ' and γ ″co-precipitation phenomena in directly aged Alloy 718 with high δ-phase fractions, Mater. Des. 241 (2024) 112961.
[11] K. Hou, M. Wang, M. Ou, H. Li, X. Hao, Y. Ma, Effects of microstructure evolution on the deformation mechanisms and tensile properties of a new Ni-base superalloy during aging at 800°C, J. Mater. Sci. Technol. 68 (2021) 40–52.
[12] D.M. Collins, H.J. Stone, A modelling approach to yield strength optimisation in a nickel-base superalloy, Int. J. Plast. 54 (2014) 96–112.
[13] J. Chen, J. Dong, M. Zhang, Z. Yao, Deformation mechanisms in a fine-grained Udimet 720LI nickel-base superalloy with high volume fractions of γ' phases, Mater. Sci. Eng. A. 673 (2016) 122–134.
[14] P.E. Aba-Perea, T. Pirling, P.J. Withers, J. Kelleher, S. Kabra, M. Preuss, Determination of the high temperature elastic properties and diffraction elastic constants of Ni-base superalloys, Mater. Des. 89 (2016) 856–863.
[15] P. Beardmore, On the temperature dependence of the flow stress of nickel-base alloys, Trans. Metall. Soc. AIME 245 (1969) 1537–1545.
[16] R. C. Reed, C. M. F. Rae, Physical metallurgy of the nickel-based superalloys, in: D. E. Laughlin, K. Hono, Physical metallurgy, 2014, pp. 2215-2290.
[17] K. Gopinath, A.K. Gogia, S.V. Kamat, R. Balamuralikrishnan, U. Ramamurty, Tensile properties of Ni-based superalloy 720Li: Temperature and strain rate effects, Metall. Mater. Trans. A. 39 (2008) 2340–2350.
[18] K. Gopinath, A.K. Gogia, S.V. Kamat, U. Ramamurty, Dynamic strain ageing in Ni-base superalloy 720Li, Acta Mater. 57 (2009) 1243–1253.
[19] A. Devaux, B. Picqué, M.F. Gervais, E. Georges, T. Poulain, P. Héritier, AD730 - a new nickel-based superalloy for high temperature engine rotative parts, Superalloys 2012 (2012) 911–919.
[20] Z. Wan, L. Hu, Y. Sun, T. Wang, Z. Li, Hot deformation behavior and processing workability of a Ni-based alloy, J. Alloys Compd. 769 (2018) 367–375.
[21] X. Wang, C. Huang, B. Zou, H. Liu, H. Zhu, J. Wang, Dynamic behavior and a modified Johnson–Cook constitutive model of Inconel 718 at high strain rate and elevated temperature, Mater. Sci. Eng. A. 580 (2013) 385–390.
[22] T.J. Jackson, J. Rolph, R.C. Buckingham, M.C. Hardy, The Effect of Shot Peening on the Ductility and Tensile Strength of Nickel-Based Superalloy Alloy 720Li, Superalloys 2020 (2020) 535–545.
[23] K. Yuan, W. Guo, P. Li, Y. Zhang, X. Li, X. Lin, Thermomechanical behavior of laser metal deposited Inconel 718 superalloy over a wide range of temperature and strain rate: Testing and constitutive modelling, Mech. Mater. 135 (2019) 13–25.
[24] T. Özel, Experimental and finite element investigations on the influence of tool edge radius in machining nickel-based alloy, Int. Manufactu. Sci. Eng. Conf. 43611 (2009) 493–498.
[25] E. Farabi, V.V. Rielli, F. Godor, C. Gruber, A. Stanojevic, B. Oberwinkler, S. Primig, New insights into the kinetics of dynamic and post-dynamic softening in Alloy 718 engine disks, Mater. Des. 247 (2024) 113423.
[26] D. Medlin, H. Kuhn, ASM Handbook. Volume 8: Mechanical Testing and Evaluation. 2000.
[27] L. Zhang, Thermo-mechanical characterization and dynamic failure of a CoCrFeNi high-entropy alloy, Mater. Sci. Eng. A. 844 (2022) 143166.
[28] A. Sela, G. Ortiz-de-Zarate, D. Soler, G. Germain, L. Gallegos, P.J. Arrazola, Adiabatic self-heating determination for Ti6Al4V at different temperatures, Int. J. Heat Mass Transf. 204 (2023) 123747.
[29] R.L. Goetz, S.L. Semiatin, The adiabatic correction factor for deformation heating during the uniaxial compression test, J. Mater. Eng. Perform. 10 (2001) (2001) 710–717.
[30] J. L. Smith, Full-Field Measurement of the Taylor-Quinney Coefficient in Tension Tests of Ti-6Al-4V, Aluminum 2024-T351, and Inconel 718 at Various Strain Rates, Ph.D. Thesis, The Ohio State University, 2019.
[31] J. Varga, O.T. Kingstedt, An investigation of the plastic work to heat conversion of wrought and laser powder bed fusion manufactured Inconel 71, Addit. Manuf. 46 (2021) 102179.
[32] C. Bonk, M. Vucetic, A. Bouguecha, B.A. Behrens, An Experimental-numerical method to determine the plastic work converted into heat applied on AHSS, Adv. Mater. Res. 1140 (2016) 51–58.
[33] P. Knysh, Y.P. Korkolis, Determination of the fraction of plastic work converted into heat in metals, Mech. Mater. 86 (2015) 71–80.
[34] S.I. Oh, S.L. Semiatin, J.J. Jonas, An analysis of the isothermal hot compression test, Metall. Mater. Trans. A. 23 (1992) 963–975.
[35] H. Monajati, M. Jahazi, R. Bahrami, S. Yue, The influence of heat treatment conditions on γ' characteristics in Udimet® 720, Mater. Sci. Eng. A. 373 (2004) 286–293.
[36] B.B. Dash, S. Dixit, C.J. Boehlert, M. Sundararaman, S. Sankaran, Influence of interrupted ageing on the temporal evolution of the γ' size distribution and the co-precipitation of γ ″in alloy 718Plus, Mater. Charact. 206 (2023) 113394.
[37] R. Ran, Y. Wang, F. Ren, Y.X. Zhang, F. Fang, W. Zhang, G. Yuan, G. Wang, Ultra-high strength Inconel 718 alloy produced by a novel heat treatment, Trans. Nonferrous Met. Soc. China. 34 (2024) 2204–2218.
[38] A. Madariaga, G. Ortiz-de-Zarate, P.J. Arrazola, Non-destructive procedure to determine residual stresses and white layers in hole making operations, NDT Int. 151 (2025) 103304.

[39] P.J. Arrazola, T. Özel, D. Umbrello, M. Davies, I.S. Jawahir, Recent advances in modelling of metal machining processes, CIRP Ann. 62 (2013) 695–718.
[40] S.N. Melkote, W. Grzesik, J. Outeiro, J. Rech, V. Schulze, H. Attia, P.J. Arrazola, R. M'Saoubi, C. Saldana, Advances in material and friction data for modelling of metal machining, CIRP Ann. 66 (2017) 731–754.
[41] W. Xiong, J. Lohmar, M. Bambach, G. Hirt, A new method to determine isothermal flow curves for integrated process and microstructural simulation in metal forming, Int. J. Mater. 8 (2015) 59–66.
[42] R. Usamentiaga, P. Venegas, J. Guerediaga, L. Vega, J. Molleda, F.G. Bulnes, Infrared thermography for temperature measurement and non-destructive testing, Sensors 14 (2014) 12305–12348.
[43] R.B. Figueiredo, M. Kawasaki, T.G. Langdon, Seventy years of Hall-Petch, ninety years of superplasticity and a generalized approach to the effect of grain size on flow stress, Prog. Mater. Sci. 137 (2023) 101131.
[44] R.C. Reed, M.P. Jackson, Y.S. Na, Characterization and modeling of the precipitation of the sigma phase in UDIMET 720 and UDIMET 720Li, Metall. Mater. Trans. A. 30 (1999) 521–533.
[45] Z. Wan, L. Hu, Y. Sun, T. Wang, Z. Li, Y. Zhang, Effect of solution treatment on microstructure and tensile properties of a U720LI Ni-based superalloy, Vacuum 156 (2018) 248–255.
[46] M.P. Jackson, R.C. Reed, Heat treatment of UDIMET 720Li: the effect of microstructure on properties, Mater. Sci. Eng. A. 259 (1999) 85–97.
[47] R. Radis, M. Schaffer, M. Albu, G. Kothleitner, P. Pölt, E. Kozeschnik, Multimodal size distributions of γ' precipitates during continuous cooling of UDIMET 720 Li, Acta Mater. 57 (2009) 5739–5747.
[48] M. Azarbarmas, M. Aghaie-Khafri, J.M. Cabrera, J. Calvo, Dynamic recrystallization mechanisms and twining evolution during hot deformation of Inconel 718, Mater. Sci. Eng. A. 678 (2016) 137–152.
[49] P.S.M. Jena, J.K. Sahu, S. Tripathy, S.K. Pradhan, B. Mahato, N. Paulose, Influence of texture on anomalous yielding behavior of thermomechanically processed nickel-based superalloy 720Li, Acta Mater. 281 (2024) 120369.
[50] N. Saunders, Phase diagram calculations for Ni-based superalloys, Superalloys 1996 (1996) 543–561.
[51] A.S. Agazhanov, D.A. Samoshkin, Y.M. Kozlovskii, Thermophysical properties of Inconel 718 alloy, J. Phys. Conf. Ser. 1382 (2019) 1–7.
[52] D. Basak, R.A. Overfelt, D. Wang, Measurement of specific heat capacity and electrical resistivity of industrial alloys using pulse heating techniques, Int. J. Thermophys. 24 (2003) 1721–1733.
[53] M. Saez-de-Buruaga, P. Aristimuño, D. Soler, E. D'Eramo, A. Roth, P.J. Arrazola, Microstructure based flow stress model to predict machinability in ferrite–pearlite steels, CIRP Ann. 68 (2019) 49–52.
[54] H. Shang, P. Wu, Y. Lou, J. Wang, Q. Chen, Machine learning-based modeling of the coupling effect of strain rate and temperature on strain hardening for 5182-O aluminum alloy, J. Mater. Process. Technol. 302 (2022) 117501.
[55] R.K. Rai, J.K. Sahu, N. Paulose, D.C. Fernando, Tensile deformation micro-mechanisms of a polycrystalline nickel base superalloy: From jerky flow to softening, Mater. Sci. Eng. A. 807 (2021) 140905.
[56] Y. Wang, W.Z. Shao, L. Zhen, L. Yang, X.M. Zhang, Flow behavior and microstructures of superalloy 718 during high temperature deformation, Mater. Sci. Eng. A. 497 (2008) 479–486.
[57] D.L. Foley, M.I. Latypov, X. Zhao, J. Hestroffer, I.J. Beyerlein, L.E. Lamberson, M. L. Taheri, Geometrically necessary dislocation density evolution as a function of microstructure and strain rate, Mater. Sci. Eng. A. 831 (2022) 142224.
[58] X.Y. Li, H.P. Zhang, J.M. Bai, X.K. Li, J. Jia, C.S. Liu, Y.W. Zhang, J.T. Liu, The evolution of γ' precipitates and hardness response of a novel PM Ni-based superalloy during thermal exposure, J. Alloys Compd. 942 (2023) 168757.
[59] F. Xue, A. Bezold, N. Volz, A. Kirchmayer, C.H. Zenk, S. Neumeier, M. Göken, Influence of the γ' Volume Fraction on the High-Temperature Strength of Single Crystalline Co–Al–W–Ta Superalloys, Crystals 13 (2023) 1095.
[60] A. Bezold, N. Volz, F. Xue, M. Göken, S. Neumeier, Anomalous work hardening behavior of a single crystalline Co-base superalloy, Alloys. 1 (2022) 243–253.
[61] A. Suzuki, T.M. Pollock, High-temperature strength and deformation of γ/γ' two-phase Co–Al–W-base alloys, Acta Mater. 56 (2008) 1288–1297.
[62] A.H.I. Mourad, A. Almomani, I. Ahmad Sheikh, A.H. Elsheikh, Failure analysis of gas and wind turbine blades: a review, Eng. Fail. Anal. 146 (2023) 107107.
[63] L. Li, S. Bi, Y. Sun, Risk assessment method for aeroengine multiple failure risk using Monte Carlo simulation, Multidiscip. Model. Mat. Struct. 12 (2016) 384–396.
[64] H. Lu, W. Zhang, Y. Chen, Y. Zhai, W. Wang, H. Long, A. Li, X. Han, Structural degradation and elemental variations in an ex-service first-stage gas turbine blade, Mater. Charact. 196 (2022) 112596.
[65] I. Dempster, W.D. Cao, R. Kennedy, B. Bond, J. Aurrecoechea, M. Lipschutz, Structure and property comparison of Allvac® 718Plus™ alloy and Waspaloy forgings, Superalloys. 718 (2005) 625–706.
[66] M.C. Hardy, M. Detrois, E.T. McDevitt, C. Argyrakis, V. Saraf, P.D. Jablonski, J. A. Hawk, R.C. Buckingham, H.S. Kitaguchi, S. Tin, Solving recent challenges for wrought Ni-base superalloys, Metall. Mater. Trans. A. 51 (2020) 2626–2650.
[67] D.Y. Pimenov, L.R.R. da Silva, A.R. Machado, P.H.P. França, G. Pintaude, D. R. Unune, M. Kuntoglu, G.M. Krolczyk, A comprehensive review of machinability of difficult-to-machine alloys with advanced lubricating and cooling technique, Tribol. Int. 196 (2024) 109677.